Colloidal and polymeric contributions to the yielding of dense microgel suspensions

Colloidal and polymeric contributions to the yielding of dense microgel suspensions

M.A. Lara-Peña[1,2], A. Licea-Claverie[3], I. Zapata-González[3] and M. Laurati[1*]

[1]Dipartimento di Chimica & CSGI, Università di Firenze, 50019 Sesto Fiorentino, Italy

[2]División de Ciencias e Ingenierías, Universidad de Guanajuato, 37150 León, Mexico

[3]Centro de Graduados e Investigación en Química del Tecnológico Nacional de México/Instituto Tecnológico de Tijuana, 22500 Tijuana, Mexico

Abstract

Hypothesis: Soft microgel colloids can be densely packed since particle networks can compress and interpenetrate. This evolution of the particle's internal structure associated with packing is expected to determine the linear viscoelastic properties and the yielding behavior of dense suspensions of microgel colloids.
Experiments: We investigated the volume fraction-dependent linear and non-linear rheological response of suspensions of soft core-shell particles formed by a poly(*N*-isopropylacrylamide) (PNIPAM) microgel core and a thin poly(ethylene glycol) (PEG) shell.
Findings: The linear viscoelasticity of suspensions reveals a transition from a fluid to a jammed glass state. Increasing volume fraction within the jammed state, the linear storage modulus and the yield stress show distinct regimes associated with the evolution of particle contacts, which involve progressive compression and interpenetration of the shell and core. The yielding of jammed suspensions occurs in two-steps: At small strains jammed cages are rearranged, while full disentanglement of interpenetrating networks only occurs at large deformations and results in fluidization. Yield strains and stresses increase with increasing shear rate or frequency, suggesting a progressive dominance of the timescale associated with shear over that associated with the internal dynamics of the system.

1. Introduction

The rheology of colloidal suspensions is of primary importance for the processing of food, solid inks, building materials such as cement, ceramic pastes, among others [1], [2]. The use of model colloidal particles has provided the opportunity to investigate the microscopic origin of the rheological response of suspensions and how this can be tailored by manipulating particle microstructure and interactions. For hard sphere-like colloids, a large degree of fundamental understanding has been achieved through a microscopic description of the effects of shear on structure [3 – 8], Brownian diffusion [9 – 13], hydrodynamics [13, 14], also for non-equilibrium states [15]. The response of soft colloids, which include emulsions and nanoemulsions, micelles, liposomes, dendrimers, star polymers, core-shell particles, microgels and others, is even richer due to the complex internal structure of these systems [16].

Among soft colloids microgel particles, in particular based on poly(*N*-isopropylacrylamide) (PNIPAM), have recently attracted considerable interest because of the broad range of technological applications [17], and because of their use as a versatile model system for fundamental studies [18]. Microgel particles have a complex internal architecture consisting of a cross-linked hydrogel network which is swollen in good solvents, making them deformable and highly compressible [18 – 20]. The cross-linking density plays an important role in determining the degree of allowed deformation and compression [21, 22]. Depending on the synthesis method and the solvent used, they may also present dangling ends which form a polymer or brush-like shell [23, 24], which is in turn compressible and penetrable [25]. The rheological response of suspensions of microgel particles has been investigated in detail in experiments [26 – 33] and models connecting the single particle properties to the suspension response have been proposed, including linear viscoelastic properties [24, 34] and flow behavior [35]. These models describe the effects of particle compression and interpenetration on the suspension rheology. Only recently the structural evolution of particles as a function of concentration has been investigated by means of zero-average contrast Small Angle Neutron Scattering (SANS) [25] or microscopy [36 – 39] and directly linked to the linear viscoelasticity [37]. In particular different regimes of the dependence of the linear storage modulus G' on concentration have been associated with the corresponding evolution of particle contacts. Such evolution also reflects the variations of the inter-particle interactions in the overlapping regime [40]. Much less is known about the effects of such structural evolution on the non-linear response and yielding [41].

More complex soft core-shell architectures have been also developed [42] to fulfill application requirements. For instance, in biomedical applications additional shells with specific ligands have been added to stimulate cell targeting [43], or to improve in general the biocompatibility of the particles [44]. The rheological behavior of suspensions of such microgel core-fuzzy shell particles is largely unexplored. In

particular, the contribution of an additional soft corona with different viscoelastic properties needs to be determined, especially for large packing fractions where particle interpenetration and deformation plays a major role. For this purpose, in this work the linear and non-linear rheological response of soft core-shell particles was investigated, where a lightly cross-linked PNIPAM microgel sphere forms the core, and pending long poly(ethylene glycol) (PEG) chains form the corona. Results on linear viscoelasticity and steady state stress during flow show the presence of three different regimes of the response as a function of particle concentration, evidencing thus the presence of an additional regime compared to the behavior commonly reported for PNIPAM microgel particles. These regimes are interpreted as being associated with the progressive compression and interpenetration of the corona and core of the particles with increasing particle concentration, with the third regime corresponding to core compression. The complex yielding of dense suspensions evidences contributions from entropic caging, typical of colloidal systems, but also from the overlapping polymeric coronas.

2. Materials and Methods:

Samples

The particles used in this work consist of a thermosensitive core, made by a crosslinked network of PNIPAM, and a shell of PEG. A schematic representation of the microgels is shown in Fig. 1a. In the reaction stage, due to their hydrophilic character, the PEG chains stabilize the emulsion and form a shell around the PNIPAM core. It has been seen that the addition of PEG to a crosslinked NIPAM microgel improves colloidal stability and hydrophilicity in particular at high temperatures, reduces the particle size, increases polydispersity and shifts the volumetric phase transition temperature (VPTT) to high temperatures [44, 45]. The synthesis details are summarized below.

All the reagents used are from Sigma Aldrich. N-isopropylacrylamide (M_n 113.16 g/mol) was purified by recrystallization in petroleum ether at 35°C. The crosslinker ethylene glycol dimethacrylate (EGDMA), the initiator ammonium persulfate (APS) (M_n 228.18 g/mol) and poly(ethylene glycol) methyl ether methacrylate (PEGMA) (M_n 950 g/mol) were used as purchased.

The core shell microgels were synthesized with a soap-free emulsion polymerization method [44] using a 1L jacketed glass reactor (Syrris, model Atlas Potassium, Royston, U.K.) to improve temperature and stirring control. The particles were synthesized with a weigh proportion of 30% of PEG and 70% PNIPAM. First, 3.5g of PNIPAM were dissolved in 40ml of water and mixed with the crosslinker (1 mol% vs PNIPAM). The solution was bubbled with nitrogen for 30 minutes to remove any dissolved oxygen while stirred at 350 rpm in a cold bath at 15°C.

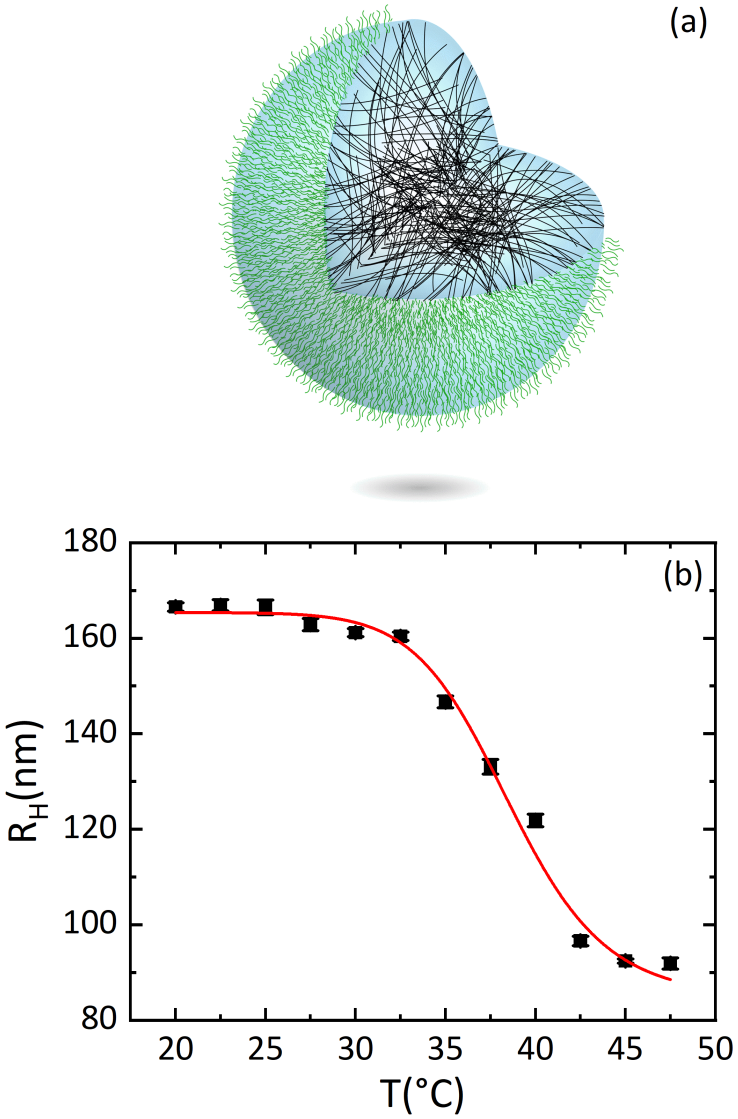

Figure 1. a) Schematic representation of a PNIPAM-PEG colloid. The non-uniform crosslinked network of PNIPAM is represented as black lines while the PEG chains are showed as green lines located on the surface of the particle. In the swollen state, the particle is filled with water, represented by blue color. b) Temperature dependence of the hydrodynamic radius of PNIPAM-PEG particles in water obtained by DLS (symbols). The solid red line represents a fit of the data with a logistic function.

After 20 minutes, 1.5g of PEG pre-dissolved in 10ml of water were added and the bubbling was maintained for 10 additional minutes. The so-obtained mixture was added to 438 ml of pre-heated water (85°C) and stirred at 350 rpm for 30 minutes. APS (2 wt% vs PNIPAM) previously dissolved in 12 ml of water was added to initiate the reaction. The polymerization was carried on for 45 minutes, after which the solution was placed in a cold bath to stop the polymerization process. The dispersion was purified via dialysis for 7 days and the colloidal particles were recovered by freeze drying. The effective weight fractions of PNIPAM and PEG in the resulting particles was confirmed by Nuclear Magnetic Resonance (NMR) measurements. Transmission Electron Microscopy (TEM) and NMR measurements performed in previous work on

samples obtained with the same synthetic procedure confirmed the core-shell structure of the particles [44,45]. The PEG corona increases the stability of the particles against aggregation even at high temperatures [45].

The microgels were redispersed in water at 0.2 wt/wt% and characterized via Dynamic Light Scattering (DLS) using a NanoBrook 90Plus Particle Size Analyzer (Brookhaven Instruments Corporation). The temperature dependent hydrodynamic radius (R_H) was determined in the range 20 °C < T < 47.5 °C after equilibrating the sample for 6 minutes at each temperature and is shown in Fig. 1b. The polydispersity of the system was estimated from the DLS measurements as $p \approx 0.19$. By assuming an ideal brush configuration (good solvent conditions) for the PEG chains formed by $n = 21$ monomers, and using the PEG monomer length $l = 0.35$ nm, the thickness of the PEG shell (dilute conditions) can be estimated as $L = n \cdot l = 7.35$ nm. Calculating the PNIPAM core surface as $A_{PNIPAM} = 4\pi R_{PNIPAM}^2$ with $R_{PNIPAM} = R_H - L = 158.65$ nm and estimating the area occupied by a PEG chain on the core through the Flory area $A_F = \pi R_F^2 = \pi n^{6/5} l^2$, where $R_F = n^{3/5} l$ is the Flory radius of the polymer in solution [46], one can estimate that approximately 2.1 x 10^4 PEG chains are grafted onto the PNIPAM core.

A series of samples with concentrations equal to 7.09, 10.43, 14.83, 17.54, 21.05, 24.5, 28.03, 31.5 and 35 wt/wt% was prepared. In all cases particles were dispersed in a 0.233 mM NaCl aqueous solution to screen electrostatic charges [28]. The correct mass of particles and solvent (water) was weighed and mixed with a small magnetic stirrer until complete homogenization was obtained. The effective volume fractions (ϕ_{eff}) of the samples at 20°C were determined according to $\phi_{eff}(T) = \phi_w [D(T)/D_{min}]^3$ [47], with T the temperature, $\phi_w = \frac{m_{coll}}{m_{coll} + m_{solv}}$ the colloid weight fraction being m_{coll} and m_{solv} the mass of the colloids and solvent, respectively, and D_{min} the minimum diameter of the particles in the collapsed state at high temperature**.** The diameter at T = 20 °C and in the collapsed state was determined by modeling the temperature dependence of the particle's diameter with a logistic function (Fig. 1b). The effective volume fractions for the samples at T = 20 °C are $\phi_{eff}(T = 20\ ℃) = 0.49, 0.73, 0.97, 1.22, 1.46, 1.71, 1.95, 2.20, 2.44$. In what follows we will indicate for simplicity $\phi_{eff}(T = 20\ ℃)$ as ϕ_{eff}.

Rheology

All measurements were carried out with a DHR-3 (TA Instrument) stress-controlled rheometer using a cone-plate geometry with a 40 mm diameter and a cone angle of 0.5081°. The absence of significant wall slip effects for samples with $\phi_{eff} > 0.49$ was confirmed by measuring the gap dependent viscosity of the samples using a 20 mm smooth plate-plate geometry. For $\phi_{eff} = 0.49$ instead indications of wall slip effects were present and a cross-hatched plate-plate geometry with diameter 40 mm was used. For the sample with $\phi_{eff} = 0.73$ a 20 mm diameter plate-plate geometry was

used. Temperature was controlled using a Peltier lower plate and the temperature was fixed to 20°C. To avoid evaporation, a solvent trap which isolates the sample from the surroundings was used. It consists of an enclosure with a solvent seal at the top and a permanent seal al the bottom which creates a saturated atmosphere.
In case of the two lowest concentrations, instead of using a solvent trap evaporation was avoided by filling the gap surrounding the geometry with mineral oil. A rejuvenation protocol was implemented before each measurement to minimize the effects of sample loading and aging. First, oscillatory shear in the form of a dynamic time sweep with a large strain amplitude (100% $< \gamma_0 <$ 700%, depending on sample) was applied for 180s. At the end of this test all samples showed a liquid-like behavior. Subsequently, the samples were subjected again to oscillatory shear in the form of a dynamic time sweep with a low strain amplitude (0.05% $< \gamma_0 <$ 0.2%, depending on sample) until a steady state in the viscoelastic moduli was reached. For all samples we found that 180s were sufficient to reach the steady state. In both dynamic time sweeps corresponding to the two steps of the rejuvenation procedure the frequency used was $\omega = 10$ rad/s.

3. Results

A. Linear Viscoelasticity

Linear viscoelastic moduli obtained from frequency sweeps (Fig. 2a, data for ϕ_{eff} = 1.22, 1.71 and 2.20 were omitted for clarity) show a solid-like response for ϕ_{eff} > 0.7 , indicated by a storage modulus G' larger than the loss modulus G'' for all measured frequencies, while a fluid-like response (G'' > G') is observed for smaller effective volume fractions. The fluid-like samples exhibit at low frequencies a weak dependence on ω of both moduli, which differs from that expected for simple Newtonian fluids ($G' \sim \omega^2$ and $G'' \sim \omega$). In the solid-like samples the gap between G' and G'' increases with decreasing frequency but no clear minimum of G'' is observed in the measured frequency range, suggesting a long relaxation time for the system. The gap also increases with increasing particle volume fraction, consistent with a slower relaxation and a longer-lived solid state. The plot of the storage modulus extracted for two fixed frequencies $\omega = 1$ and 10 rad/s (G'_1 and G'_{10} , respectively) as a function of the effective volume fraction ϕ_{eff} (Fig. 2b) indicates the presence of distinct regimes: For $\phi_{eff} \lesssim 0.7$ we observe a smooth increase of the modulus, which can be associated with the approach to the fluid-solid transition already discussed for Fig. 2a.
For $0.7 \leq \phi_{eff} <$ 2.0 the modulus shows a sharper increase, which can be described with a linear dependence $G' \sim A(\phi_{eff} - \phi_c)$, with $A = 32$ and 60 Pa for $\omega = 1$ and 10 rad/s, respectively, and $\phi_c = 0.684$ in both cases. Finally, for ϕ_{eff} > 2.0 the increase of G' is more pronounced and can be described with a power-law $G' \sim (\phi_{eff})^{\beta}$ with $\beta \approx$ 8.4.

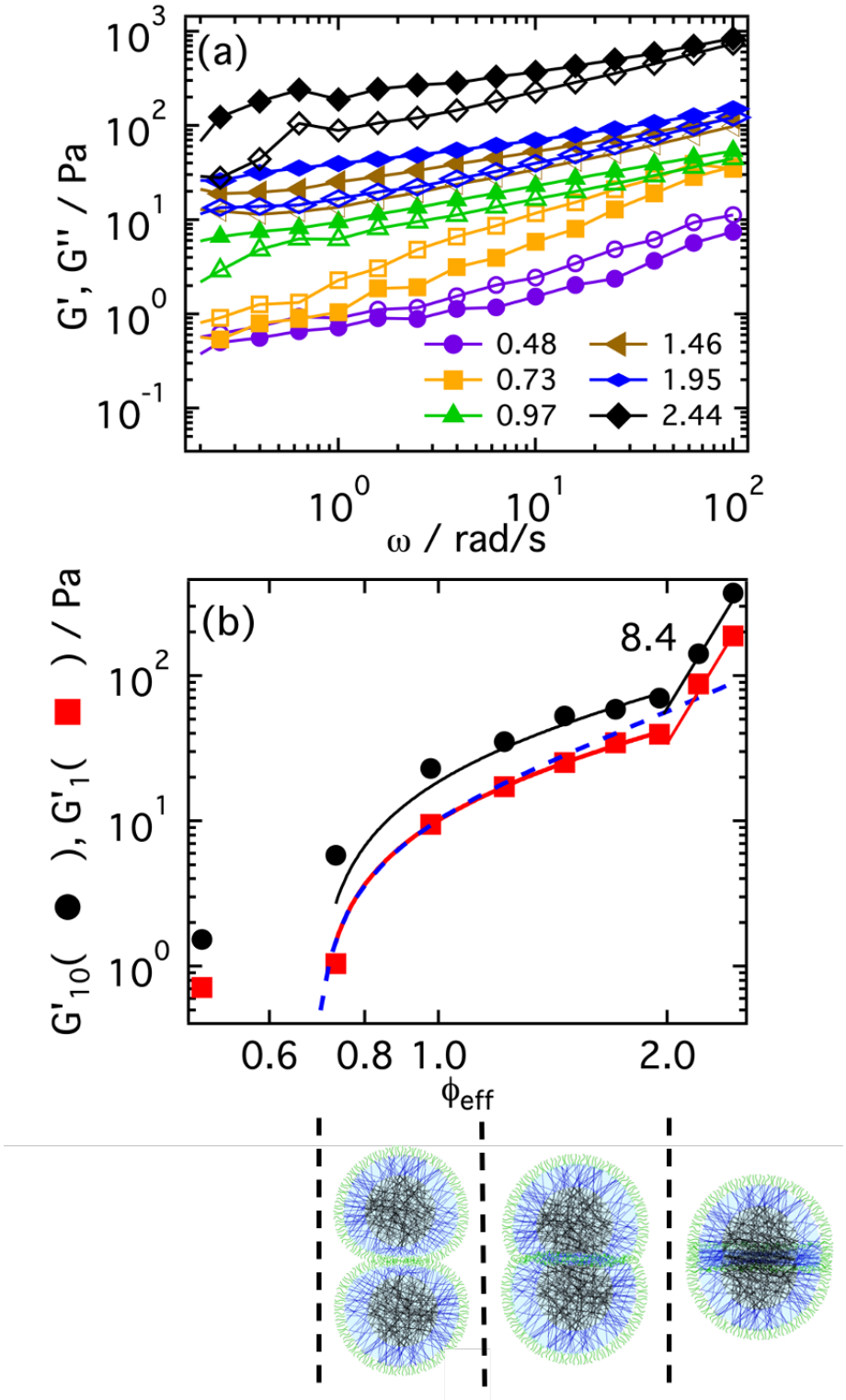

Figure 2: a) Dynamic frequency sweeps at different values of ϕ_{eff}, as indicated. Solid symbols represent the elastic moduli, *G'*, and open symbols the viscous moduli, *G''*. b) Storage modulus at $\omega = 10$ rad/s (G'_{10}) and $\omega = 1$ rad/s (G'_1) as a function of ϕ_{eff} . The solid lines for $\phi_{eff} < 2.0$ represent linear dependencies $G' \sim A(\phi_{eff} - \phi_c)$. The dashed blue line represents the dependence of G' on ϕ_{eff} predicted by the model of [37]. The solid lines for $\phi_{eff} > 2.0$ show power-law dependencies with the indicated exponent 8.4. Bottom: Schematic representation of the interaction regimes between two colloidal particles. The dense crosslinked PNIPAM core is represented in black color, while the fuzzy PNIPAM shell, characterized by a smaller density and crosslinking degree, is represented in blue color. Finally, the PEG external corona is represented in green color. For $0.64 < \phi_{eff} < 1.2$, the PEG coronas

and external PNIPAM layers are in contact and deform. For $1.2 < \phi_{eff} < 2.0$ interpenetration of the internal PNIPAM cores takes place. For $\phi_{eff} > 2.0$, core interpenetration reaches a limit and core compression occurs.

The exact value of the power-law exponent for ϕ_{eff} > 2.0 is only indicative due to the small number of data points in this regime. Note that trends for different frequencies are completely consistent, in particular for $\phi_{eff} > 0.8$. The linear dependence observed for intermediate values of ϕ_{eff} agrees with previous results for PNIPAM microgel suspensions [24, 34, 37, 41, 48] and dense star polymer solutions [49] in the jammed glass regime corresponding to ϕ_{eff} > 1. On the other hand, the storage modulus of polystyrene (PS) particles covered with a PNIPAM shell shows a stronger power law dependence on ϕ_{eff} [49]. It is interesting to note that comparing to results in [48], our data suggest a behavior closer to that of star polymers than to PS-PNIPAM core-shell colloids and compared to results in [24], our data show agreement with particles having a smaller degree of crosslinking. These comparisons suggest a particularly soft, star-like internal structure of the PNIPAM-PEG particles, in particular the PNIPAM core, which has been confirmed by SANS experiments [50].
In [37] the rheological response of dense suspensions was connected to variations of the internal structure of the microgels. The microgels studied in [24, 37] present an internal structure similar to that described for our system: They are composed of a dense core and a fuzzy, brush-like corona: in the regime $0.64 < \phi_{eff} < 1$ the fuzzy shells of the particles are in contact. The increase of the storage modulus was interpreted in terms of the progressive compression of the shells making use of a combination of rheology and super-resolution microscopy. A schematic representation of the corona interaction in this regime for the PNIPAM-PEG particles of this work is reported in Fig. 2b (bottom). The increase of G' is described using a model of brush-like interactions between the particle coronas. The input parameters of the model are the size ratio between the core radius R_c and the total radius R_t, $\alpha = R_c/R_t$, and the jamming volume fraction, ϕ_J, of the suspension: $G' \sim B(\tau^{9/4} - \tau^{-3/4})$, where $\tau = (1-\alpha)/[\left(\phi_{eff}/\phi_J\right)^{-1/3} - \alpha]$ and B is a prefactor which depends on the grafting density of the corona and is typically fitted to the data. Fig. 2b reports a model calculation obtained for our system (dashed blue line), for which we used $\alpha = 0.47$ according to SANS measurements which indicate $R_c \approx 78$ nm as obtained by a Guinier fit of the low Q-range of the particle form factor [50], and $R_t = 166$ nm obtained from DLS measurements (details in the "Materials and Methods" section). For ϕ_J, the value of $\phi_c = 0.684$ was used at which the onset of the linear dependence of G' on ϕ_{eff} is observed. Using B = 12 Pa the model is consistent with the data for $\phi_{eff} \lesssim 1.2$. Considering that the studied particles have a degree of cross-linking which is about 5 times smaller than particles in [37], it appears reasonable that the model describes the experimental data to larger ϕ_{eff} (also in agreement with results in [24]). In the regime of $\phi_{eff} > 1.2$ coronas collapse and the internal cores of the particles

interpenetrate and deform [36] (Fig. 2b, bottom): The softness of the core dominates and leads to a linear increase of the modulus with increasing effective volume fraction. The good agreement between the data obtained in this investigation and results reported in [24,37] concerning the ϕ_{eff} dependence of G' and its modeling indicates that a structural evolution comparable to that described in [37] can be assumed for the PNIPAM-PEG system.

Interestingly, these data present an additional response regime at the highest effective volume fractions, which has not been reported for PNIPAM microgels. In this additional regime, as observed previously, the increase of the modulus as a function of ϕ_{eff} is particularly pronounced. For $\phi_{eff} > 2$ microscopy observations in [37] suggest the saturation of core interpenetration and the onset of isotropic compression: One might therefore interpret the sharp increase of the modulus in the final regime as associated to isotropic compression of the cores that have reached saturation of interpenetration (Fig. 2b, bottom). A multi-Hertzian potential has been recently introduced to describe the interactions of particles with a core-corona structure analogous to that of the colloids used in this study [40]. This potential combines Hertzian interactions of increasing strength to describe corona-corona, core-corona and core-core interactions and has been used to explain the structural evolution of binary mixtures of PNIPAM particles. The model of the interactions proposed in [40] is consistent with the increasingly stronger dependence of G' on ϕ_{eff} observed in the PNIPAM-PEG system.

B. Steady state stresses

Fig. 3a shows stresses measured in flow curves for various values of ϕ_{eff}. Samples with the lowest volume fractions, ϕ_{eff} = 0.49 and 0.73, show a fluid-like response with the stress increasing approximately linearly with the shear rate $\dot{\gamma}$. Instead for $\phi_{eff} \geq 0.97$ all curves show the typical behavior of a yield stress fluid, with a sub-linear increase of the stress as a function of applied shear rate and the presence of a finite yield stress for $\dot{\gamma} \to 0$. Flow curves were measured starting from the largest value and decreasing the shear rate: The asymptotic value at small rates can be thus interpreted as a dynamic yield stress. This is consistent with the solid-like nature of the dispersions also evidenced by the Dynamic Frequency Sweeps. The curves move to higher values of the stress with increasing ϕ_{eff} , except for samples with ϕ_{eff} = 1.46, 1.71 and 1.95, which show values similar with each other. These values correspond to the regime for which $G' \sim \phi_{eff}$. Flow curves for $\phi_{eff} \geq 0.97$ were modeled using a Herschel-Bulkley (HB) type relation, $\sigma = \sigma_y + k(\dot{\gamma})^{\nu}$, obtaining values of the yield stress σ_y and of the high rate power-law exponent ν. The dependence of the fitted values of σ_y on ϕ_{eff} will be discussed in section 3.D together with results obtained from transient tests.

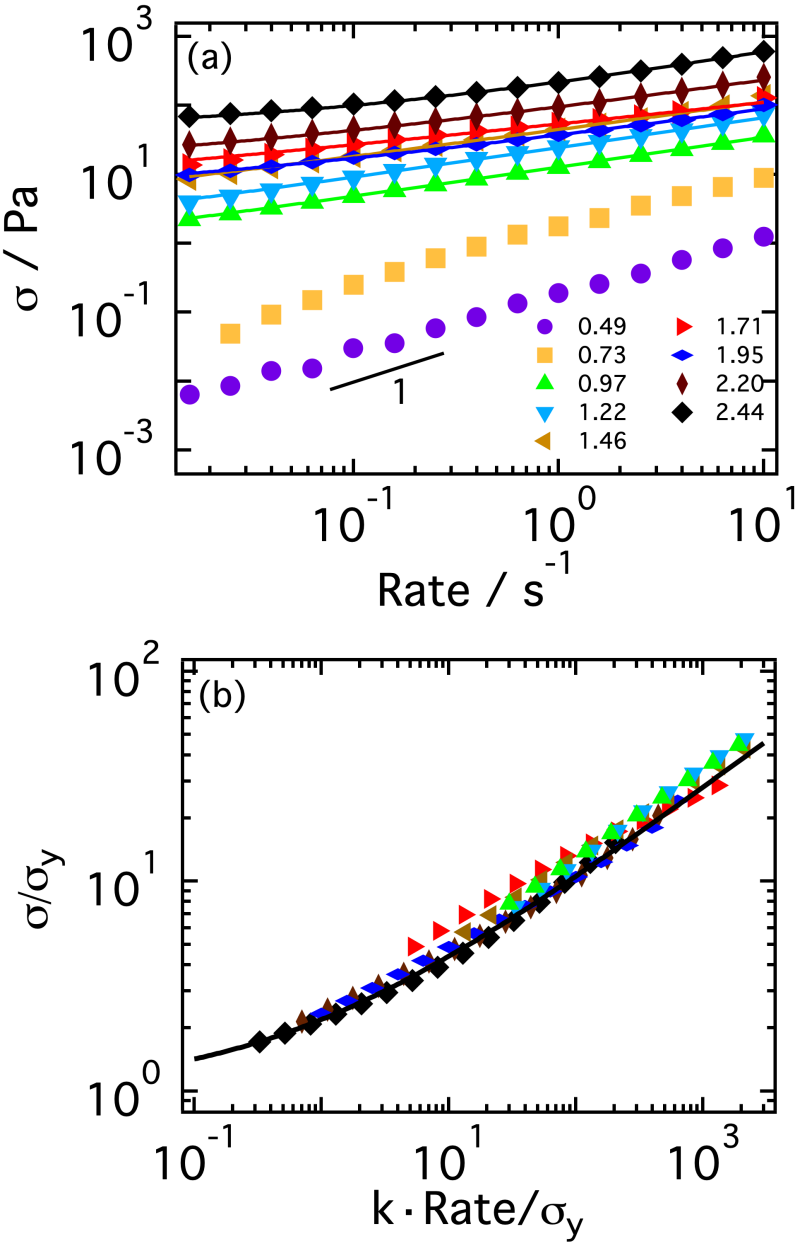

Figure 3: a) Stress σ as a function of shear rate $\dot{\gamma}$, measured in flow curves for samples corresponding to different values of ϕ_{eff}, as indicated. Lines are fits to a Herschel-Bulkley (HB) type relation. b) Scaled stress σ/σ_y as a function of scaled shear rate $k\dot{\gamma}/\sigma_y$ obtained from flow curves of samples corresponding to different values of ϕ_{eff}, same symbols as in a). Values of σ_y and k where obtained from the fits in a). The solid line is a generalized Herschel-Bulkley fit of the form $\sigma/\sigma_y = 1 + A\left(k\dot{\gamma}/\sigma_y\right)^{1/2}$

The exponents ν present values in the range $0.4 \leq \nu \leq 0.5$ which are in agreement with previous results on soft spheres [41, 52]. It has been proposed that a value of $\nu = 0.5$ is characteristic of the flow of soft particles exhibiting inter-particle slippage in dense dispersions under shear [35, 52, 53].

It was tested whether the flow curve data for samples showing a solid-like response can be interpreted in terms of a micromechanical model proposed to describe the rheological behavior of jammed soft glasses [35]. The model describes the behavior of

a dispersion of elastic spheres with contact modulus E^* being compressed and forming facets with several different neighbors. According to the model, the flow curves of different samples should follow a master curve if plotted in terms of a scaled stress, σ/σ_y , versus a scaled shear rate $k\dot{\gamma}/\sigma_y$, where k and σ_y are obtained from the HB fits presented in Fig. 3a. The scaled stress vs. scaled rate curves are reported in Fig. 3b. The scaling works relatively well for samples with the largest effective volume fraction $\phi_{eff} = 1.95$, 2.20 and 2.44, while significant deviations are observed for the lower values $\phi_{eff} = 0.97, 1.22, 1.46, 1.71$. The line in Fig. 3b is a prediction $\sigma/\sigma_y = 1 + A\left(k\dot{\gamma}/\sigma_y\right)^{1/2}$ for a value A = 1.19, which describes relatively well the data with larger ϕ_{eff}. The ϕ_{eff} dependence of G' indicates that isotropic core compression effects might take place for $\phi_{eff} > 2$: since compression and deformation effects are the basic assumption of the model described in [35], this could explain the better agreement between experimental data and the model in the regime of large ϕ_{eff}. Instead, for the lower values of ϕ_{eff} interpenetration of the corona and core, effects which are not considered in the model, should play an important role.

C. Transient Response

The yielding transition of samples with $\phi_{eff} \geq 0.97$, i.e. samples which respond as viscoelastic solids at rest, was investigated through different rheological measurements: step rate tests, oscillatory amplitude sweeps and creep tests. Yielding is typically associated with a rearrangement of the microstructure of the samples induced by shear. Fig. 4a shows stress (σ) versus strain (γ) curves obtained from step rate experiments for samples with different ϕ_{eff} and one shear rate $\dot{\gamma}$ = 0.1 s^{-1}. Data for additional shear rates for selected samples are reported in the Supporting Material, Fig. S1. For all samples, the qualitative behavior is similar: The stress σ initially increases with increasing γ, until a first inflection is observed in the range $20\% < \gamma < 40\%$, depending on ϕ_{eff}. After the inflection, σ increases again and a stress overshoot for strains $300\% < \gamma < 2000\%$ (depending on ϕ_{eff}) is observed. While a steady state value of the stress is not clearly attained in most cases, values at the largest strains are in good agreement with results of flow curves. Moreover, it was not observed any indication of a sudden stress decay from the plateau value, which is a signature of shear induced layering or crystallization in dense suspensions of microgel particles [51]. The inflection and the overshoot are indicative of yielding processes. A stress overshoot is characteristic of the yielding of many different materials and in particular of dense colloidal suspensions formed by hard and soft spheres as well as star polymers [4, 5, 8, 11, 49, 54–60]. For such systems it has been associated with cage deformation, leading to accumulation of stress, followed by cage breaking and stress release.

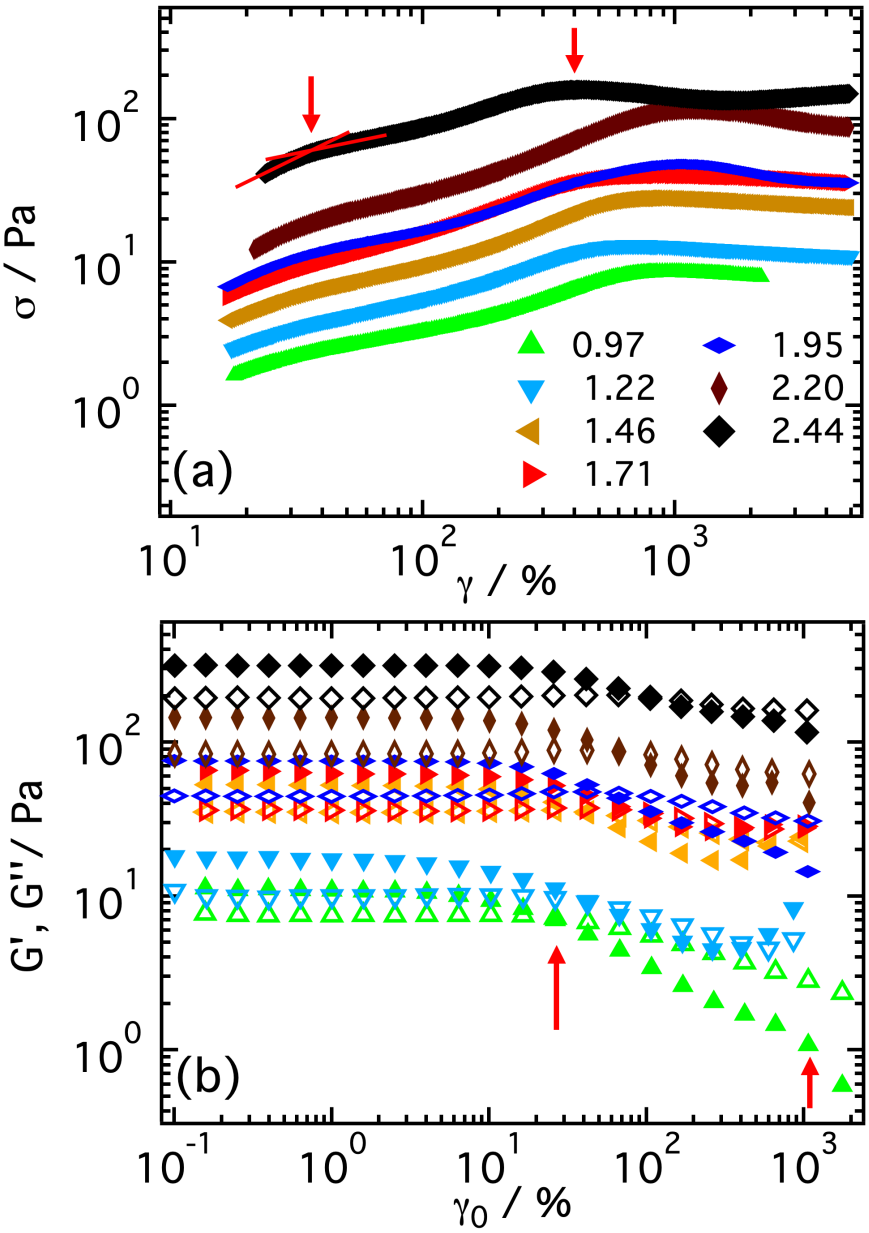

Figure 4: Non-linear rheological tests for samples with different values of $\boldsymbol{\phi_{eff}}$, as indicated. (a) Stress versus strain curves measured in Step Rate experiments for $\dot{\boldsymbol{\gamma}} = \mathbf{0.1}$ s^{-1}. (b) Storage (G') and Loss (G'') moduli measured in Amplitude Sweeps, as a function of strain amplitude $\boldsymbol{\gamma_0}$, for an oscillation frequency $\boldsymbol{\omega} = \mathbf{1}$ rad/s.

The characteristic strains associated with the overshoot are in those cases of the order of the relative cage deformation, i.e. $10\% < \gamma < 100\%$. Such values correspond to the first inflection of the stress vs strain curves in Fig.4a, while the stress overshoot is observed at significantly larger values of γ. This suggests that the first inflection of the stress, rather than the overshoot, corresponds to initial cage deformation. The fact that we observe an inflection rather than a maximum suggests that cages are not entirely broken at this stage. This might be the result of temporary entanglements associated with the contacts between coronas and cores of the particles, which do not

allow particles to escape cage confinement. Entanglement effects in interpenetrating brushes and how their lifetime is affected by shear have been described in the literature [61]. Due to the entanglements, the cage can deform further without breaking, until the strain is sufficiently large to fully disentangle the chains of neighboring particles and release them from cages. It can be speculated that this occurs at the second yield point, where an overshoot is observed. As an alternative picture, stress release at large deformations might be associated with the relaxation of polymer deformation at the interface between two jammed particles. Strong deformation of loosely cross-linked microgel particles at a solid interface, leading to a strong increase in the monomer density at the interface and polymer elongated deformation, have been reported recently [62]. Formation of a similar interface might occur when two microgel particles are jammed together: Shear advection could then lead to a relaxation of the local polymer elongation and recoiling, resulting in stress release.

Data in Fig. 4a additionally show a qualitative difference between samples with $\phi_{eff} \geq 1.95$ and samples with lower effective volume fractions: While the overshoot is relatively sharp for the higher ϕ_{eff} samples, it is particularly broad for the low values. This seems to be associated with the different regimes of the interaction evidenced in the values of the storage modulus and yield stress presented in the previous sections (Fig.2). In particular one might speculate that for intermediate values of ϕ_{eff} the degree of corona overlap still allows a certain dynamic of the polymer chains, and disentanglement might be partially opposed by re-formation of temporary crosslinks. On the other hand, for the higher ϕ_{eff} samples particles are strongly compressed and interpenetrated, and coronas fully collapsed, therefore polymer dynamics become less important and a more sudden disentanglement is observed. Note that star-like micelles show a qualitative behavior with a certain similarity, i.e. the presence of particularly broad overshoots [49]. It was also observed that the broad overshoots are mainly present at low and intermediate shear rates (see Supporting Material, Fig. S1). This is coherent with the interpretation of the ϕ_{eff} dependence: when the timescale associated with shear, $1/\dot{\gamma}$, becomes sufficiently short compared to relaxation processes in the overlapping coronas, the overshoot becomes sharper.

Oscillatory Amplitude Sweeps confirm the presence of a two-step yielding behavior. In these tests it was only determined the frequency dependent storage and loss moduli in first harmonic approximation, which provides a qualitative information on the dependence of the yielding process on the control parameters, in particular the relative volume fraction ϕ_{eff} and the oscillation frequency ω. More detailed information on the contribution of higher harmonics and in-cycle processes can be obtained by LAOS analyses [63, 64], which will be the subject of a separate study. Fig. 4b shows the storage (G') and loss (G'') moduli obtained from measurements at $\omega =$

1 rad/s, as a function of the strain amplitude γ_0. For all samples the moduli are approximately constant up to strain amplitudes of a few percent, while for larger values of γ_0 the storage modulus G' starts to decrease and the loss modulus G'' increases, until a crossing point of the moduli for amplitudes $20\ \% < \gamma_{cross} < 50\%$ is observed. This crossing point indicates a partial fluidization of the system and thus a first yield point. For larger deformations both moduli decrease as a function of γ_0, up to strain amplitudes in the range $500\% < \gamma_0 < 2000\%$, where an inflection (samples with $\phi_{eff} = 0.97, 1.95, 2.20, 2.44$) or a second crossing followed by a sharp increase of G' (samples with $\phi_{eff} = 1.22, 1.46, 1.71$) is observed. The inflection or crossing point is indicating a second yield point, in agreement with the findings of step rate experiments. The response of samples with ϕ_{eff} = 1.22 and 1.46 (and to a minor extent ϕ_{eff} = 1.71) is particularly interesting due to the second crossing of the moduli and the following sharp increase of G', which suggest the onset of shear thickening. In these samples with intermediate values of the colloid volume fraction it is speculated that particle cores might interpenetrate and form temporary entanglements. The incomplete release and stretching of entanglements might lead to a thickening phenomenon at sufficiently large oscillatory amplitudes.

D. Yield Strain and Stress

Values of the yield strains and stresses were extracted from step rate and amplitude sweep experiments. Yield stresses were also extracted from flow curves. For step rates the strain values were determined corresponding to the first inflection of the stress (γ_1) and the stress overshoot (γ_2) for different shear rates. They are reported in Fig. 5a as a function of the relative volume fraction ϕ_{eff}. The first yield strain γ_1 presents only moderate variations as a function of ϕ_{eff}, mostly observed for the smallest shear rate, $\dot{\gamma} = 0.01$ s^{-1}, where γ_1 initially decreases attaining a minimum for ϕ_{eff} = 1.46, and after increases. For $\dot{\gamma} = 0.1$ and 1.0 s^{-1} the variations are less pronounced and indicate a slight increase for the larger values of ϕ_{eff}. The first yield strain increases for all samples with increasing shear rate. Note that for the highest rate the value of $\gamma_1$falls out of the measurement window and therefore could not be determined.
In Fig. 5a values are reported of the first yield strain γ_{cross} extracted from Amplitude Sweeps in Fig.4b ($\omega = 1$ rad/s). As it can be seen the absolute values and the qualitative dependence on ϕ_{eff} are consistent with those of γ_1, indicating that the same yielding phenomena are observed in the different rheological tests. As discussed earlier, the first yield process can be interpreted as associated with cage deformation. The poor volume fraction dependence of $\gamma_1(\gamma_{cross})$ might be the result of the fact that for all investigated volume fractions particles are highly packed, exceeding random close packing. Therefore, in all samples we have cages of jammed particles: the amount of strain needed to break a jammed cage should be comparable at fixed shear

rate and the different values of ϕ_{eff} are linked to a different degree of particle compression/deformation within the jammed cage.

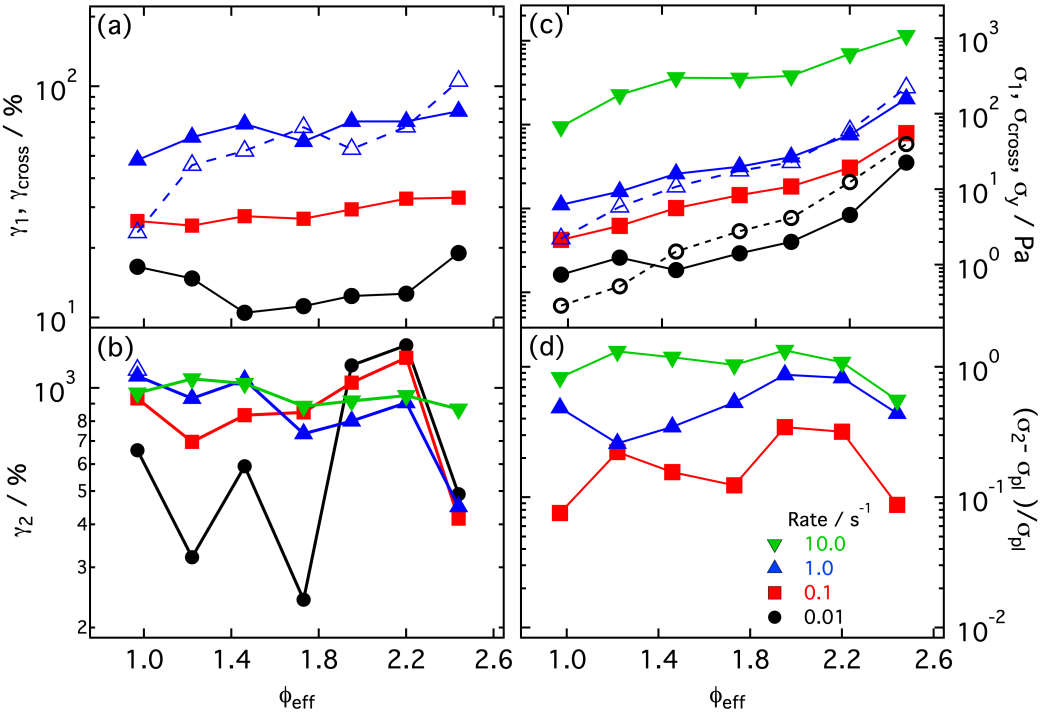

Figure 5: Parameters extracted from step rate and oscillatory Amplitude Sweep experiments, as a function of ϕ_{eff}. Data from step rate experiments are reported for different shear rates $\dot{\gamma}$, as indicated in the legend. Data from Amplitude Sweeps are reported for $\omega = 1$ rad/s. (a) First yield strain from step rate tests (γ_1, full symbols) and yield strain corresponding to the first crossing of G' and G'' from amplitude sweep tests (γ_{cross}, empty symbols). (b) Second yield strain from step rate tests (γ_2, full symbols). The value of the second yield strain obtained in amplitude sweep tests for $\phi_{eff} = 0.97$ is also reported (empty symbol). (c) Yield stress from HB fits of flow curves (σ_y, open circles), first yield stress from step rate tests (σ_1, full symbols), stress at which G' and G'' from amplitude sweep tests first cross (σ_{cross}, empty triangles). (d) Relative height of the stress overshoot $(\sigma_2 - \sigma_{pl})/\sigma_{pl}$, where σ_2 is the value of the stress at the overshoot and σ_{pl} is the value of the stress at the longest time, approaching the steady state value.

The increase of γ_1 with increasing shear rate can be explained as the result of the increasing dominant contribution of affine deformations imposed by shear at higher rates, which allow larger cage deformations since particle dynamics cannot contribute to cage release. Note that also for γ_{cross} we observe a similar dependence on oscillation frequency (not shown).

The second yield strain γ_2 (Fig. 5b) shows larger variations with ϕ_{eff} for the smallest shear rate, in particular evidencing a maximum value larger than 1000% for the sample with ϕ_{eff} = 2.20. Such large fluctuations might be associated with the noise in the signal at small rates. While a maximum is still present for $\dot{\gamma} = 0.1$ s^{-1}, for larger rates γ_2 is almost constant up to ϕ_{eff} = 2.20. In all cases γ_2 decreases for the largest value of ϕ_{eff}. Also, the rate dependence shows qualitative differences: The value of γ_2 increases with increasing $\dot{\gamma}$ for the lower ϕ_{eff} , otherwise it decreases for the larger.

As discussed previously, we interpret the strain γ_2 in terms of the deformation needed to finally disentangle neighbor particles and lead to final cage breakup and a transition to flow. Following this interpretation, one might understand the increase of the yield strain with increasing ϕ_{eff} (up to 2.20) as the effect of stronger and longer-lived entanglements due to increasing particle interpenetration with increasing ϕ_{eff}. Additionally, the increase with $\dot{\gamma}$ might be associated with the fact that at low rates some disentanglement might be facilitated by the internal dynamics of the particles, while at high shear rates these dynamics become irrelevant. The final drop might be associated to the foreseen transition to a regime in which the particle core starts to be deformed and the system's response tends to approach that of a hard sphere suspension.

The yield stresses obtained from different tests are reported in Fig.5c. While σ_y and σ_{cross} can be considered dynamic yield stresses, σ_1 rather represents a static yield stress. All yield stresses show comparable trends, they increase with increasing ϕ_{eff} and indicate the presence of different regimes similar to those observed for G'. In particular the yield stress increases faster for the smaller and larger values of ϕ_{eff}, where compression effects are dominant, and slower for intermediate values, where corona and core interpenetration occur. This confirms that the evolution of the particle microstructure as a function of ϕ_{eff} also affects the non-linear response. Quantitative differences are expected between different rheological tests [65], consistent with our findings. Fig. 5d reports the relative height of the stress overshoot, $(\sigma_2 - \sigma_{pl})/\sigma_{pl}$, where σ_{pl} represents the value of the stress at the maximum strain, i.e. approaching the steady state. This quantity indicates the amount of stress stored during the yielding process. One can see that the trend of the relative height of the overshoot as a function of ϕ_{eff} is relatively similar to that of γ_2, with a maximum around $\phi_{eff} = 1.97, 2.20$. It also increases for all samples with increasing $\dot{\gamma}$. The two results seem to be consistent with the interpretation proposed for γ_2: With increasing volume fraction larger deformations are needed to release particles, leading to a larger stress accumulation before yielding.

Since yielding of glassy and jammed suspensions is sensitive to the application of strain or stress [59, 66], additionally the response of the system in step stress (creep) tests was investigated. As shown in Figs. S2 and S3 of the Supporting Material, also in creep tests a complex yielding behavior was observed, which is coherent with that found in the strain-controlled tests. At intermediate and large applied stresses, after an initial super-linear increase associated with tool inertia, the strain increases in a sub-linear fashion at short times, presents an inflection at intermediate times and finally approaches a linear dependence characteristic of a flowing system at long times, eventually through a super-linear regime. The inflection at intermediate times indicates a first yield process, but longer application of the stress is needed to induce flow in the system. A similar behavior characterized by two yield points has been observed for systems such as gels and attractive glasses [10, 57, 67].

4. Conclusions

The experimental investigation of the linear and non-linear rheological responses of dense suspensions of soft core-shell particles composed of a microgel core and a fuzzy PEG corona revealed a complex dependence on the suspension effective particle volume fraction. We observed a fluid-solid transition which can be associated with jamming and results in a sharp increase of the elastic modulus. In the jammed regime our data on the storage modulus can be described with a model which determines the dispersion elasticity on the basis of brush-brush interactions [34, 36, 37] that result in corona compression and interpenetration. In the case of our system, such brush interactions involve both the PEG corona and the fuzzy external shell of the PNIPAM spheres. For larger volume fractions another regime is observed where the modulus shows an approximately linear increase with increasing ϕ_{eff}, which has been associated with core interpenetration and deformation [37]. At the largest investigated packing fractions an additional regime is observed, where the modulus increases again sharply. We interpret this regime as being associated with saturated particle interpenetration and the beginning of compression of the PNIPAM cores. Such compression effects have been observed in PNIPAM microgel particles [36, 37] and DNA-based colloids [68], but their effects on the rheology have not been reported. The yield stress extracted from flow curves of solid-like samples shows similar regimes. A micromechanical model proposed for PNIPAM homogeneous microgels [35] seems to describe well the flow properties of samples in which compression effects are dominant but is less accurate for describing samples in which interpenetration effects are important. This supports our structural interpretation of the different regimes. Transient yielding under continuous shear evidences the presence of two yielding processes, one occurring at strains in the range 10%-100%, which we associate to entropic cage deformation, and another occurring at large strains of the order of a few 100% or larger. The second yielding process can be interpreted as the deformation needed to fully disentangle the interpenetrated neighbor particles forming a cage structure. Contributions of polymer dynamics in the overlapping coronas seem to influence the speed of stress release after the overshoot. Indications of such two-step yielding process are also found in oscillatory amplitude sweep and creep tests. In all cases the yield strains and stresses increase with increasing shear rate, indicating the increasing dominance of the timescale imposed by shear over the internal dynamics of the system.

Results from this investigation show that in dense suspensions of soft particles with complex internal microstructures the flow behavior is also complex and is characterized by different regimes, which reflect the combination of colloidal and polymeric behavior and the microstructural evolution of the particle structure with

increasing packing density. The full understanding of such complex response needs to be linked in detail to the particle structural evolution through scattering and/or microscopy.

5. Acknowledgments

We acknowledge fruitful discussions with J.M. Ruiz-Franco and A. Pamvouxoglou. M. L.-P. and M.L. acknowledge support from the project “A1-S-9098” funded by Conacyt within the call “Convocatoria de Investigación Básica 2017-2018” and from “Consorzio per lo Sviluppo dei Sistemi a Grande Interfase” (CSGI).

References

[1] J. Mewis and N. J. Wagner, *Colloidal Suspension Rheology*. Cambridge University Press, New York, 2012.

[2] R. G. Larson, *The structure and rheology of complex fluids*. Oxford university press New York, 1999.

[3] X. Cheng, J. H. McCoy, J. N. Israelachvili, and I. Cohen, “Imaging the Microscopic Structure of Shear Thinning and Thickening Colloidal Suspensions,” *Science*, vol. 333, no. 6047, p. 1276, Sep. 2011, doi: 10.1126/science.1207032.

[4] N. Koumakis *et al.*, “Start-up shear of concentrated colloidal hard spheres: Stresses, dynamics, and structure,” *J. Rheol.*, vol. 60, no. 4, pp. 603–623, 2016, doi: http://dx.doi.org/10.1122/1.4949340.

[5] N. Koumakis, M. Laurati, S. U. Egelhaaf, J. F. Brady, and G. Petekidis, “Yielding of Hard-Sphere Glasses during Start-Up Shear,” *Phys. Rev. Lett.*, vol. 108, no. 9, p. 98303, Mar. 2012, doi: 10.1103/PhysRevLett.108.098303.

[6] C. P. Amann, D. Denisov, M. T. Dang, B. Struth, P. Schall, and M. Fuchs, “Shear-induced breaking of cages in colloidal glasses: Scattering experiments and mode coupling theory,” *J. Chem. Phys.*, vol. 143, no. 3, p. 34505, 2015, doi: http://dx.doi.org/10.1063/1.4926932.

[7] J. Zausch *et al.*, “From equilibrium to steady state: the transient dynamics of colloidal liquids under shear,” *J. Phys.: Condens. Matter*, vol. 20, p. 404210, 2008.

[8] M. Laurati, P. Masshoff, K. J. Much, S. U. Egelhaaf, and A. Zaccone, “Long-lived neighbors determine the rheological response of glasses,” *Phys. Rev. Lett.*, vol. 118, p. 18002, 2016.

[9] R. Besseling, E. R. Weeks, A. B. Schofield, and W. C. K. Poon, “Three-Dimensional Imaging of Colloidal Glasses under Steady Shear,” *Phys. Rev. Lett.*, vol. 99, no. 2, p. 28301, Jul. 2007, doi: 10.1103/PhysRevLett.99.028301.

[10] T. Sentjabrskaja *et al.*, “Creep and flow of glasses: strain response linked to the spatial distribution of dynamical heterogeneities,” *Sci. Rep.*, vol. 5, p. 11884, 2015.

[11] T. Sentjabrskaja *et al.*, “Transient dynamics during stress overshoots in binary colloidal glasses,” *Soft Matter*, vol. 10, pp. 6546–6555, 2014.

[12] N. Koumakis *et al.*, “Start-up shear of concentrated colloidal hard spheres: Stresses, dynamics, and structure,” *J. Rheol.*, vol. 60, no. 4, pp. 603–623, 2016, doi: 10.1122/1.4949340.

[13] D. R. Foss and J. F. Brady, “Structure, diffusion and rheology of Brownian suspensions by Stokesian Dynamics simulation,” *J. Fluid Mech.*, vol. 407, pp. 167–200, 2000, doi: 10.1017/S0022112099007557.

[14] J. Bergenholtz, J. F. Brady, and M. Vicic, “The non-Newtonian rheology of dilute colloidal suspensions,” *J. Fluid Mech.*, vol. 456, pp. 239–275, 2002, doi: DOI: 10.1017/S0022112001007583.

[15] J. M. Brader, “Nonlinear rheology of colloidal dispersions,” *J. Phys.: Condens. Matter*, vol. 22, no. 36, p. 363101, 2010, doi: 10.1088/0953-8984/22/36/363101.

[16] D. Vlassopoulos and M. Cloitre, “Tunable rheology of dense soft deformable colloids,” *Curr. Opin. Colloid Interf. Sci.*, vol. 19, no. 6, pp. 561–574, 2014, doi: https://doi.org/10.1016/j.cocis.2014.09.007.

[17] S. Nayak and L. A. Lyon, “Soft Nanotechnology with Soft Nanoparticles,” *Angew. Chem. Int. Ed.*, vol. 44, no. 47, pp. 7686–7708, Dec. 2005, doi: 10.1002/anie.200501321.

[18] A. Fernandez-Nieves, H. Wyss, J. Mattsson, and D. A. Weitz, *Microgel Suspensions: Fundamentals and Applications*. Wiley, 2011.

[19] R. Pelton, “Temperature-sensitive aqueous microgels,” *Adv. Coll. Interf. Sci.*, vol. 85, no. 1, pp. 1–33, 2000, doi: https://doi.org/10.1016/S0001-8686(99)00023-8.

[20] L. Rovigatti, N. Gnan, and E. Zaccarelli, “Internal structure and swelling behaviour of in silico microgel particles,” *J. Phys.: Condens. Matt.*, vol. 30, no. 4, p. 044001, 2017, doi: 10.1088/1361-648x/aaa0f4.

[21] H. Senff and W. Richtering, “Influence of cross-link density on rheological properties of temperature-sensitive microgel suspensions,” *Coll. Polym. Sci.*, vol. 278, no. 9, pp. 830–840, 2000, doi: 10.1007/s003960000329.

[22] B. Sierra-Martin and A. Fernandez-Nieves, “Phase and non-equilibrium behaviour of microgel suspensions as a function of particle stiffness,” *Soft Matter*, vol. 8, no. 15, pp. 4141–4150, 2012, doi: 10.1039/C2SM06973C.

[23] J. Brijitta and P. Schurtenberger, “Responsive hydrogel colloids: Structure, interactions, phase behavior, and equilibrium and nonequilibrium transitions of microgel dispersions,” *Curr. Opin. Colloid Interf. Sci.*, vol. 40, pp. 87–103, 2019, doi: https://doi.org/10.1016/j.cocis.2019.02.005.

[24] F. Scheffold, P. D\’{\i}az-Leyva, M. Reufer, N. ben Braham, I. Lynch, and J. L. Harden, “Brushlike Interactions between Thermoresponsive Microgel Particles,” *Phys. Rev. Lett.*, vol. 104, no. 12, p. 128304, Mar. 2010, doi: 10.1103/PhysRevLett.104.128304.

[25] P. S. Mohanty *et al.*, “Interpenetration of polymeric microgels at ultrahigh densities,” *Sci. Rep.*, vol. 7, no. 1, p. 1487, 2017, doi: 10.1038/s41598-017-01471-3.

[26] H. Senff and W. Richtering, “Temperature sensitive microgel suspensions: Colloidal phase behavior and rheology of soft spheres,” *J. Chem. Phys.*, vol. 111, no. 4, pp. 1705–1711, 1999, doi: 10.1063/1.479430.

[27] M. Stieger, J. S. Pedersen, P. Lindner, and W. Richtering, “Are Thermoresponsive Microgels Model Systems for Concentrated Colloidal Suspensions? A Rheology and Small-Angle Neutron Scattering Study,” *Langmuir*, vol. 20, no. 17, pp. 7283–7292, Aug. 2004, doi: 10.1021/la049518x.

[28] K. van der Vaart, Y. Rahmani, R. Zargar, Z. Hu, D. Bonn, and P. Schall, “Rheology of concentrated soft and hard-sphere suspensions,” *J. Rheol.*, vol. 57, no. 4, pp. 1195–1209, 2013, doi: 10.1122/1.4808054.

[29] V. Carrier and G. Petekidis, “Nonlinear rheology of colloidal glasses of soft thermosensitive microgel particles,” *J. Rheol.*, vol. 53, no. 2, pp. 245–273, Feb. 2009, doi: 10.1122/1.3045803.

[30] A. Basu *et al.*, “Rheology of soft colloids across the onset of rigidity: scaling behavior, thermal, and non-thermal responses,” *Soft Matter*, vol. 10, no. 17, pp. 3027–3035, 2014, doi: 10.1039/C3SM52454J.

[31] M. Cloitre, “Yielding, Flow, and Slip in Microgel Suspensions: From Microstructure to Macroscopic Rheology,” in *Microgel Suspensions*, John Wiley & Sons, Ltd, 2011, pp. 283–309.

[32] J. J. Liétor-Santos, B. Sierra-Martín, and A. Fernández-Nieves, “Bulk and shear moduli of compressed microgel suspensions,” *Phys. Rev. E*, vol. 84, no. 6, p. 60402, Dec. 2011, doi: 10.1103/PhysRevE.84.060402.

[33] R. Rivas-Barbosa *et al.*, “Different routes into the glass state for soft thermo-sensitive colloids,” *Soft Matter*, vol. 14, no. 24, pp. 5008–5018, 2018, doi: 10.1039/C8SM00285A.

[34] G. Romeo and M. P. Ciamarra, “Elasticity of compressed microgel suspensions,” *Soft Matter*, vol. 9, no. 22, pp. 5401–5406, 2013, doi: 10.1039/C3SM50222H.

[35] J. R. Seth, L. Mohan, C. Locatelli-Champagne, M. Cloitre, and R. T. Bonnecaze, “A micromechanical model to predict the flow of soft particle glasses,” *Nature Materials*, vol. 10, no. 11, pp. 838–843, 2011, doi: 10.1038/nmat3119.

[36] G. M. Conley, P. Aebischer, S. Nöjd, P. Schurtenberger, and F. Scheffold, “Jamming and overpacking fuzzy microgels: Deformation, interpenetration, and compression,” *Sci. Adv.*, vol. 3, no. 10, p. e1700969, Oct. 2017, doi: 10.1126/sciadv.1700969.

[37] G. M. Conley, C. Zhang, P. Aebischer, J. L. Harden, and F. Scheffold, “Relationship between rheology and structure of interpenetrating, deforming and compressing microgels,” *Nat. Commun.*, vol. 10, no. 1, p. 2436, 2019, doi: 10.1038/s41467-019-10181-5.

[38] S. Bergmann, O. Wrede, T. Huser, and T. Hellweg, “Super-resolution optical microscopy resolves network morphology of smart colloidal microgels,” *Phys. Chem. Chem. Phys.*, vol. 20, no. 7, pp. 5074–5083, 2018, doi: 10.1039/C7CP07648G.

[39] A. P. H. Gelissen *et al.*, “3D Structures of Responsive Nanocompartmentalized Microgels,” *Nano Letters*, vol. 16, no. 11, pp. 7295–7301, Nov. 2016, doi: 10.1021/acs.nanolett.6b03940.

[40] M.J. Bergman, N. Gnan, M. Obiols-Rabasa, J.-M. Mejier, L. Rovigatti, E. Zaccarelli and P. Schurtenberger, “A new look at effective interactions between microgel particles”. *Nat. Commun.* 9, 5039 (2018), https://doi.org/10.1038/s41467-018-07332-5

[41] C. Pellet and M. Cloitre, “The glass and jamming transitions of soft polyelectrolyte microgel suspensions,” *Soft Matter*, vol. 12, no. 16, pp. 3710–3720, 2016, doi: 10.1039/C5SM03001C.

[42] C. D. Jones and L. A. Lyon, “Synthesis and Characterization of Multiresponsive Core−Shell Microgels,” *Macromolecules*, 33, 22, pp. 8301–8306, Oct. 2000, doi: 10.1021/ma001398m.

[43] S. Nayak, H. Lee, J. Chmielewski, and L. A. Lyon, “Folate-Mediated Cell Targeting and Cytotoxicity Using Thermoresponsive Microgels,” *J. Am. Chem. Soc.*, vol. 126, no. 33, pp. 10258–10259, Aug. 2004, doi: 10.1021/ja0474143.

[44] A. Serrano-Medina, J. M. Cornejo-Bravo, and A. Licea-Claveríe, “Synthesis of pH and temperature sensitive, core–shell nano/microgels, by one pot, soap-free emulsion polymerization,” *J. Coll. Interf. Sci.*, vol. 369, no. 1, pp. 82–90, 2012, doi: 10.1016/j.jcis.2011.12.045

[45] J. Es Sayed, C. Lorthioir, P. Perrin and N. Sanson, “PEGylated NiPAM microgels: synthesis, characterization and colloidal stability,” *Soft Matter*, vol. 15, no. 5, pp. 963-972, 2019, doi: 10.1039/C8SM02156B.

[46] P. Flory, “Principles of Polymer Chemistry”, Cornell University Press, 1953.

[47] X. DI, X. Peng and G. B. McKenna, “Dynamics of a thermo-responsive microgel colloid near to the glass transition,”*J. Chem. Phys,* vol. 140, no. 5, p. 054903, 2014, doi: 10.1063/1.4863327.

[48] K. van der Vaart, Y. Rahmani, R. Zargar, Z. Hu, D. Bonn, and P. Schall, “Rheology of concentrated soft and hard-sphere suspensions,” *J. Rheol.*, vol. 57, no. 4, pp. 1195–1209, 2013, doi: http://dx.doi.org/10.1122/1.4808054.

[49] N. Koumakis, A. Pamvouloglou, A. S. Poulos, and G. Petekidis, “Direct comparison of the rheology of model hard and soft particle glasses,” *Soft Matter*, vol. 8, no. 15, pp. 4271–4284, 2012, doi: 10.1039/C2SM07113D.

[50] R. Rivas-Barbosa, M. Lara-Peña, J.M. Ruiz-Franco, E. Zaccarelli, and M. Laurati, “Ultrasoft architecture of core-shell microgel colloids”, In preparation.

[51] F. Khabaz, T. Liu, M. Cloitre, and R.T. Bonnecaze, “Shear-induced ordering and crystallization of jammed suspensions of soft particles glasses”, *Phys. Rev. Fluids*, 2, 093301, 2017.

[52] S. P. Meeker, R. T. Bonnecaze, and M. Cloitre, “Slip and flow in pastes of soft particles: Direct observation and rheology,” *J. Rheol.*, vol. 48, no. 6, pp. 1295–1320, Nov. 2004, doi: 10.1122/1.1795171.

[53] M. Cloitre, R. Borrega, F. Monti, and L. Leibler, “Glassy Dynamics and Flow Properties of Soft Colloidal Pastes,” *Phys. Rev. Lett.*, vol. 90, no. 6, p. 68303, Feb. 2003, doi: 10.1103/PhysRevLett.90.068303.

[54] T. Voigtmann, “Nonlinear glassy rheology,” *Curr. Opin. Coll. Interf. Sci.*, vol. 19, no. 6, pp. 549–560, 2014, doi: http://dx.doi.org/10.1016/j.cocis.2014.11.001.

[55] C. P. Amann, M. Siebenbürger, M. Krüger, F. Weysser, M. Ballauff, and M. Fuchs, “Overshoots in stress-strain curves: Colloid experiments and schematic mode coupling theory,” *J. Rheol.*, vol. 57, no. 1, pp. 149–175, 2013, doi: http://dx.doi.org/10.1122/1.4764000.

[56] L. Mohan, R. T. Bonnecaze, and M. Cloitre, “Microscopic Origin of Internal Stresses in Jammed Soft Particle Suspensions,” *Phys. Rev. Lett.*, vol. 111, no. 26, p. 268301, Dec. 2013, doi: 10.1103/PhysRevLett.111.268301.

[57] M. E. Helgeson, N. J. Wagner, and D. Vlassopoulos, “Viscoelasticity and shear melting of colloidal star polymer glasses,” *J. Rheol.*, vol. 51, pp. 297–316, 2007.
[58] M. Laurati, S. U. Egelhaaf, and G. Petekidis, “Nonlinear rheology of colloidal gels with intermediate volume fraction,” *J. Rheol.*, vol. 55, no. 3, pp. 673–706, 2011, doi: http://dx.doi.org/10.1122/1.3571554.
[59] T. Sentjabrskaja, J. Hendricks, A. R. Jacob, G. Petekidis, S. U. Egelhaaf, and M. Laurati, “Binary colloidal glasses under transient stress- and strain-controlled shear,” *J. Rheol.*, vol. 62, no. 1, pp. 149–159, 2018, doi: 10.1122/1.5009193.
[60] T. Sentjabrskaja, M. Laurati, and S. U. Egelhaaf, “One- and two-component colloidal glasses under transient shear,” *Europ. Phys. J Spec. Topics*, vol. 226, no. 14, pp. 3023–3037, Aug. 2017, doi: 10.1140/epjst/e2017-70076-0.
[61] T. A. Witten, L. Leibler, and P. A. Pincus, “Stress relaxation in the lamellar copolymer mesophase,” *Macromolecules*, vol. 23, no. 3, pp. 824–829, Feb. 1990, doi: 10.1021/ma00205a022.
[62] X. Song, C. Qiao, J. Tao, B. Bao, X. Han, and S. Zhao, “Interfacial Engineering of Thermoresponsive Microgel Capsules: Polymeric Wetting vs Colloidal Adhesion”, *Macromolecules* 52, 3869-3880, 2019.
[63] K. Hyun *et al.*, “A review of nonlinear oscillatory shear tests: Analysis and application of large amplitude oscillatory shear (LAOS),” *Prog. Polym. Sci.*, vol. 36, no. 12, pp. 1697–1753, 2011.
[64] R. H. Ewoldt, “Defining nonlinear rheological material functions for oscillatory shea,” *J. Rheol.*, vol. 57, p. 177□195, 2013.
[65] M. Dinkgreve, J. Paredes, M.M. Denn, D. Bonn, “On different ways of measuring “the” yield stress”, *J Non-Newtonian Fluid Mech*, 238, 233–241, 2016.
[66] M. Siebenbürger, M. Ballauff, and Th. Voigtmann, “Creep in Colloidal Glasses,” *Phys. Rev. Lett.*, vol. 108, no. 25, p. 255701, Jun. 2012, doi: 10.1103/PhysRevLett.108.255701.
[67] K. N. Pham, G. Petekidis, D. Vlassopoulos, S. U. Egelhaaf, W. C. K. Poon, and P. N. Pusey, “Yielding behavior of repulsion- and attraction-dominated colloidal glasses,” *J. Rheol.*, vol. 52, no. 2, pp. 649–676, 2008, doi: http://dx.doi.org/10.1122/1.2838255.
[68] J. Zhang, P. M. Lettinga, J. K. G. Dhont, and E. Stiakakis, “Direct Visualization of Conformation and Dense Packing of DNA-Based Soft Colloids,” *Phys. Rev. Lett.*, vol. 113, no. 26, p. 268303, Dec. 2014, doi: 10.1103/PhysRevLett.113.268303.